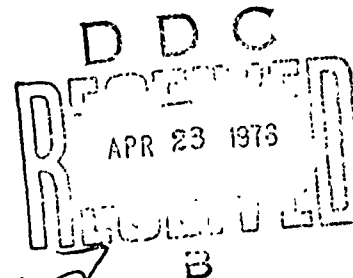# NSWC

TECHNICAL REPORT

WHITE OAK LABORATORY

PREDICTION OF VERTICAL WATER-ENTRY FORCES ON OGIVES FROM CONE DATA

BY
J.L. Baldwin

15 AUGUST 1975

NAVAL SURFACE WEAPONS CENTER
WHITE OAK LABORATORY
SILVER SPRING, MARYLAND 20910

● Approved for public release; distribution unlimited.

DDC
APR 23 1976
B

NAVAL SURFACE WEAPONS CENTER
WHITE OAK, SILVER SPRING, MARYLAND 20910

SECURITY CLASSIFICATION OF THIS PAGE *(When Data Entered)*

REPORT DOCUMENTATION PAGE		READ INSTRUCTIONS BEFORE COMPLETING FORM
1. REPORT NUMBER NSWC/WOL/TR-75-100	2. GOVT ACCESSION NO.	3. RECIPIENT'S CATALOG NUMBER
4. TITLE *(and Subtitle)* Prediction of Vertical Water-Entry Forces on Ogives from Cone Data		5. TYPE OF REPORT & PERIOD COVERED Interim rept.
		6. PERFORMING ORG. REPORT NUMBER
7. AUTHOR(s) J. L. Baldwin		8. CONTRACT OR GRANT NUMBER(s)
9. PERFORMING ORGANIZATION NAME AND ADDRESS Naval Surface Weapons Center White Oak Laboratory White Oak, Silver Spring, Maryland 20910		10. PROGRAM ELEMENT, PROJECT, TASK AREA & WORK UNIT NUMBERS ORD-035B-501/UR12-301-003
11. CONTROLLING OFFICE NAME AND ADDRESS		12. REPORT DATE 15 August 1975
		13. NUMBER OF PAGES 48
14. MONITORING AGENCY NAME & ADDRESS *(if different from Controlling Office)*		15. SECURITY CLASS. *(of this report)* Unclassified
		15a. DECLASSIFICATION/DOWNGRADING SCHEDULE

16. DISTRIBUTION STATEMENT *(of this Report)*

Approved for public release; distribution unlimited

17. DISTRIBUTION STATEMENT *(of the abstract entered in Block 20, if different from Report)*

18. SUPPLEMENTARY NOTES

19. KEY WORDS *(Continue on reverse side if necessary and identify by block number)*

Ogives, Cusps, Cones, Water entry, Vertical drag

20. ABSTRACT *(Continue on reverse side if necessary and identify by block number)*

An empirical method of predicting the drag coefficient for vertical water entry of pointed shapes is presented. The drag coefficient versus depth function is generated from experimental results of the vertical entry of cones of various angles. Comparison with experimental results shows that the predicted values are accurate to within ±25 percent. A computer program for predicting the water-entry drag coefficient of many shapes is included.
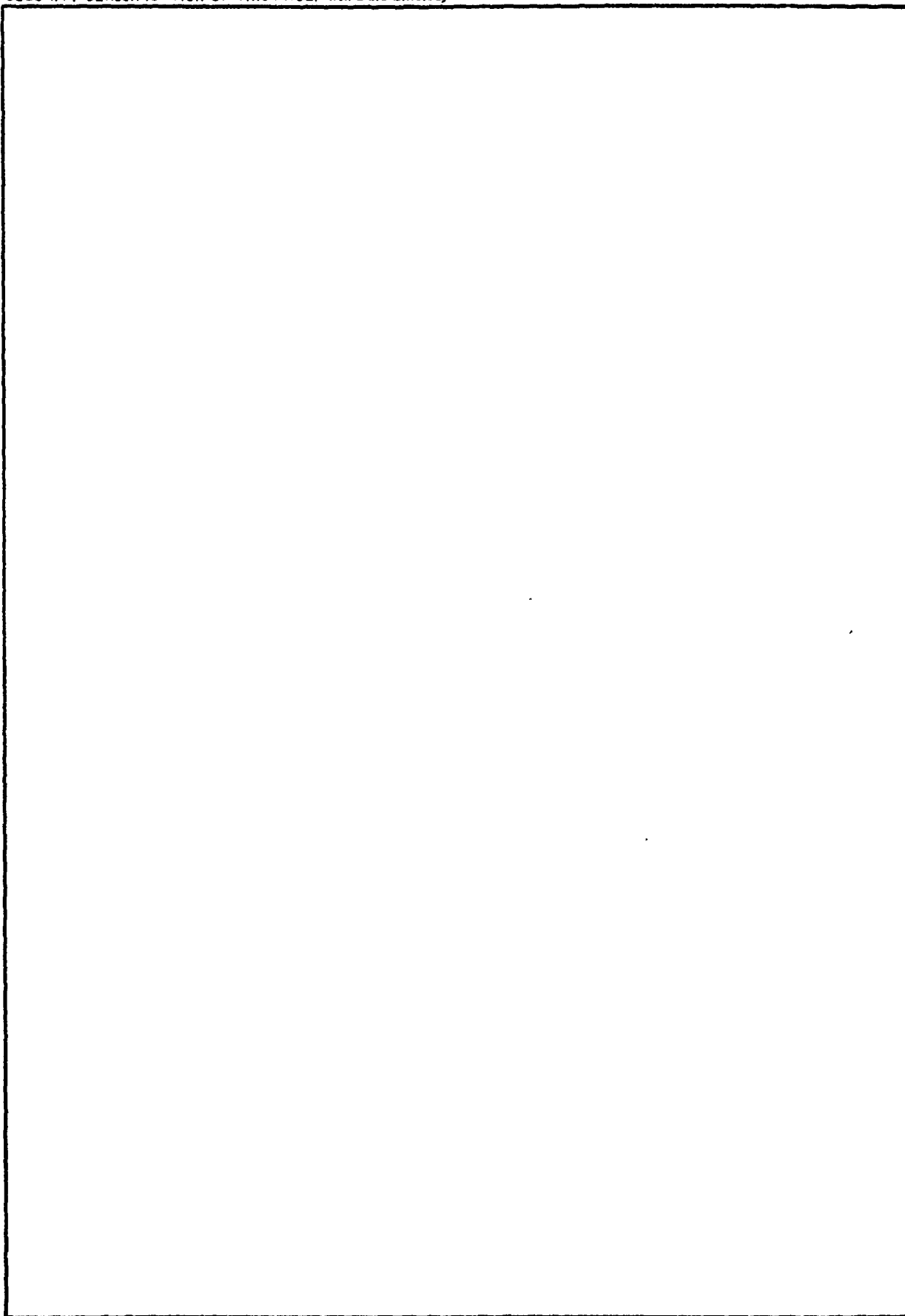
DD FORM 1 JAN 73 **1473** EDITION OF 1 NOV 65 IS OBSOLETE
S/N 0102-014-6601 |

391596

NSWC/WOL/TR 75-100   15 August 1975

PREDICTION OF VERTICAL WATER-ENTRY FORCES ON OGIVES FROM
CONE DATA

K. R. Enkenhus

K. R. ENKENHUS
By direction

CONTENTS

ILLUSTRATIONS

CONTENTS (Cont.)

TABLES

LIST OF SYMBOLS

A   Base area (πR^2)

B   Buoyancy force

C   A constant

C_d Total drag coefficient

C_{ds} Steady-state pressure drag coefficient

C_{dt} Transient drag coefficient

C_f Friction drag coefficient

D   Missile diameter

g   Gravitational constant

h   Penetration ratio $\left(\dfrac{S \text{ at maximum } C_d}{\text{cone length}}\right)$

K   Total mass constant

k   Added mass constant

L   Length

M   Missile mass

m   Added mass

R   Base radius

r   Local radius

S   Distance traveled after water contact

U   Instantaneous speed

U_o Water contact speed

α Total cone angle

β Swept angle

ρ Fluid mass density

INTRODUCTION

The two-dimensional case of water impact originally received the majority of attention due to its application to the landing of flying boats and seaplanes. Analytical prediction of the forces resulting from water entry began with a study of the landing impact of seaplane floats by von Karman in 1929 (Ref. (1)). In his paper, von Karman assumed that all the impact force was due to an increase in added mass, and that the amount of added mass was identical to one half of the added mass of a flat strip with width equal to the width of the float where intersected by the original water surface. The factor of one half was used because half of the assumed flow field was in air which contributed a negligible amount of mass to the total. In 1931, Wagner considered the effects of water-surface displacement during entry (Ref. (2)). Many subsequent investigators have also considered the problem of surface motion. Mayo in 1945 (Ref. (3)) and Pierson in 1951 (Ref. (4)) were still refining the prediction of seaplane impact. In addition to their specific contributions, they also include summaries of much of the previous work on the seaplane problem.

The prediction of the water-impact force experienced by axisymmetric bodies began as early as 1942 when Plesset applied von Karman's approach to the entry of torpedoes. In this method, the assumption was made that the added mass, "m" at any point during entry was the same as half that of a thin flat circular plate defined by the intersection of the nose and the original water surface. Half of the added mass for a disk is

$$m = 1.28 \ \rho \ \frac{\pi}{3} \ r^3 \tag{1}$$

where r is the radius and ρ is the water density. Differentiation with respect to the distance s yields:

$$\frac{dm}{ds} = (1.28) \ \rho \ \pi r^2 \ \frac{dr}{ds} \tag{2}$$

Also, the transient drag coefficient "C_{dt}" had been shown to be given by equation (3) (See Appendix A).

$$C_{dt} = \frac{2}{\rho A} \frac{dm}{ds} \tag{3}$$

Substituting equation (2) into equation (3) yields:

$$C_{dt} = \frac{2.56}{A} \ \pi r^2 \ \frac{dr}{ds} = 2.56 \left(\frac{r}{R}\right)^2 \frac{dr}{ds} \tag{4}$$

where R is the base radius and A is the base area.

5

For example, for a cone of total angle "α":

$$r = S \tan \left(\frac{\alpha}{2}\right); \quad C_{dt} = 2.56 \left(\tan \frac{\alpha}{2}\right)^3 \frac{S^2}{R^2} \quad \text{for } 0 \leq S \leq R \tan \frac{\alpha}{2}$$

$$C_{dt} = 0 \text{ for } S > \tan R \frac{\alpha}{2}$$

For a nose shape following a cubic relationship

$$r = CS^{1/3}; \quad C_{dt} = \frac{.85C^3}{R^2} \quad \text{for } 0 \leq S \leq (R/C)^3$$

$$C_{dt} = 0 \text{ for } S > (R/C)^3$$

Then $C_{dt}(S)$ was easily calculated for any desired shape; however, as the theory was developed and experimental results accumulated, several substantial deficiencies became apparent. The predicted drag coefficients for 90 and 20 degree total angle cones are compared to experimental values (Ref. (5)) in Figure 1. Experimentally derived water-entry drag coefficients for cones are also given in Reference (6)).

The drag force predicted by this method becomes equal to zero when the base of the nose passes the undisturbed water surface and remains at zero for deeper penetration. In reality, the transient axial force continues below the water surface for about a nose length before the steady-state drag coefficient is obtained.

In most cases, the predicted drag coefficient is much larger than that obtained experimentally. This over-prediction seems to be caused by the assumption that the nose shape does not affect the added mass constant. Note that this method predicts that the final added mass and hence, the change in velocity during water entry is a function of only missile diameter.

Added mass constants for the various cones were derived theoretically by Shiftman and Spencer (Ref. (7)) and experimentally (Ref. (5)). In both cases, the mass constant was equal to zero at zero cone angle and increased monotonically with increasing cone angle.

The predicted value of rise time is normally longer than experimental value. This error results from the fact that the water surface usually does not remain flat during entry as assumed.

6

It is the purpose of this report to present a simple systematic method of applying the experimental results for cones given in reference (5) to the prediction of the total drag coefficient experienced during vertical water entry by ogives and other non-flat shapes.

BACKGROUND

The basic equations for axial forces encountered during water entry are included in Appendix A, which was copied from reference (5). The identification of ogives in this report follows the method used in reference (8), each ogive shape being uniquely defined by a cone angle and a swept angle. The ogive geometry section of reference (8) is also included in Appendix A.

PREDICTION METHOD

The proposed technique for estimating the total drag coefficient of axisymmetric bodies during vertical water entry consists of predicting a friction drag coefficient, a steady-state pressure drag coefficient and a transient drag coefficient, and then summing the three functions. Or

$$C_d(S) = C_f(S) + C_{ds}(S) + C_{dt}(S) \qquad (5)$$

where each coefficient is for constant velocity entry and constant velocity cone entry data is used to calculate C_{ds} and C_{dt}. A computer program written in BASIC that performs these calculations is presented in Appendix B.

During the wetting process the water-entry force acts upon an area that extends above the original water surface as shown in Figure 2. The upper edge of this area is defined as the effective water surface and its distance from the tip of the missile is defined as the effective distance (S_{eff}). When the shape is a cone, self similar flow exists which implies that the distance from the tip to the original water surface divided by S_{eff} produces a constant. This ratio is approximated by the penetration ratio (h).

$$\frac{S \text{ at maximum } C_d}{\text{Cone Length}} = h \approx \frac{S}{S_{eff}} \qquad (6)$$

The values of penetration ratio for total cone angles between ten degrees and 140 degrees was given in reference (5).

For more general shapes the value of S_{eff} is estimated by adding the incremented effect of each body angle as it passes the original water surface as shown by

$$S_{eff} = \int_0^S \frac{ds}{h} \qquad (7)$$

where $h = f(\alpha)$ and $\alpha = g(S)$. Wetting is assumed completed when the effective distance equals the length of the nose.

The friction drag coefficient is estimated by: integrating a constant friction coefficient of .003 over the body to the effective water surface; taking the axial component and correcting the reference area to the base area of the body. This simple form was chosen so that the total drag coefficient would not be a function of entry speed and size. The addition of a varying friction coefficient could be made to the computer program subroutine beginning at line 1200 for increased accuracy for those cases that have significant friction drag.

The steady-state pressure drag coefficient is estimated to be the same as a cone with the same base diameter as the missile, undisturbed water surface diameter, and the same effective water surface body angle as the missile as illustrated in Figure 3. Addition of the friction drag coefficient to the steady-state pressure drag coefficient produces the steady-state drag coefficient which is computed up to the first maximum larger than .02. At all deeper depths the maximum value is used. When no maximum occurs on the body, the last value computed during wetting is defined as the maximum, and applied as above. In effect cavitation is predicted to begin at the depth which maximizes the steady-state drag coefficient.

The transient drag coefficient is also estimated from an equivalent cone. This cone has the same base diameter as the missile. The equivalent cone angle is the larger of the two body angles taken at the undisturbed water surface and at the effective water surface (see Figure 3). When wetting is completed the last value of transient drag coefficient and equivalent cone angle are retained in the program. At deeper depths the transient drag coefficient decays at the rate given in reference (5) for the equivalent cone angle. When the value of C_{dt} becomes smaller than two percent of C_{ds}, all calculations are terminated.

8

The calculating procedure may seem to be arbitrary and to violate accepted theory; however, it is presented as an engineering tool and during its development this method resulted in the best overall fit to available experimental data.

COMPARISON WITH EXPERIMENTS

The predicted values of the drag coefficient vs. depth function were computed for all axisymmetric shapes for which water-entry data were found. In addition, the steady-state drag coefficient was computed for all shapes for which the experimental value was found. Comparison of the calculated values with the experimental data showed that the predicted values would satisfy the accuracy requirements of most engineering applications.

The results of reference (5) were used to develop the numerical curve fits that form the core of the computing program. In order to determine the accuracy of the fitting operation, the maximum total drag coefficient, the penetration ratio and the final steady-state drag coefficient were computed for each cone angle reported in reference (5) and also for several blunter cones. The results of these calculations are compared to the experimental results in Table 1.

In the actual calculation procedure, the instantaneous drag coefficients are used; hence, it is of the utmost importance to have an accurate fit with regard to penetration ratio. An inspection of the results shows that the penetration ratio is calculated to within one percent of the experimental data for total cone angles between 20 and 140 degrees. Penetration ratios larger than unity were not allowed in the fitting process, which accounts for the large errors for the 10-and 15-degree cones. These large errors in penetration ratio for the ten and 15-degree cones caused the total maximum drag coefficient and the steady-state drag coefficient to also be lower than expected. In general, the values of calculated maximum total drag coefficients were larger than the experimental values. As indicated in reference (5), this is to be expected due to "roll off" that occurs at the peaks.

Upon discarding the values for maximum total drag coefficient for 30-degree cones, the remaining calculations and experimental values agree to within ± ten percent.

Steady-state drag coefficient values were found for ogives and paraboloids of revolution. The comparison of the experimental values at zero cavitation number and the calculated values are given in Table 2 for ogives and Table 3 for paraboloids.

9

TABLE 1

Comparison of Input and Curve Fit Results for Cones

Total Cone Angle	Cdmax Total Exp.	Fit	Fit/Exp.	Penetration Ratio Exp.	Fit	Fit/Exp.	Cds Assumed Fit	Cds Fit	Fit Assumed
10	.0574	.0556	.969	1.037	.967	.932	.0595	.0538	.904
15	.0662	.0689	1.041	1.057	.952	.901	.0684	.0642	.939
20	.0873	.095	1.088	.943	.937	.994	.0866	.0867	1.001
30	.139	.168	1.209	.906	.913	1.008	.141	.149	1.056
45	.293	.314	1.072	.886	.883	.997	.257	.258	1.004
60	.466	.511	1.097	.857	.853	.995	.365	.358	.981
90	1.178	1.245	1.057	.802	.806	1.005	.497	.501	1.008
120	2.842	2.981	1.049	.763	.758	.993	.596	.597	1.002
140	5.547	5.322	.960	.715	.719	1.006	.660	.664	1.006
160	--	10.3			.671			.740	
170	--	16.5			.640			.776	
175	--	23.3			.624			.788	
179	--	35.5			.610			.795	

TABLE 2

Comparison of Steady-State Drag Coefficient
for Tangent Ogives

Dia./R (of cavity)	α/β	Exp. C_d(max)	Ref. No.	Calculated C_d(max)	$\dfrac{\text{Cal.}}{\text{Exp.}}$	$\dfrac{\text{Cal.}}{\text{Exp.}}(\sigma=.015)$
1/2	90/90	.29	9	.338	1.166	1.166
1	60/60	.195+.209σ .1515+.595σ .22	10 11 12			
	Average	.189		.212	1.122	1.098
1.5	48.2/48.2	.14	13	.161	1.15	1.15
2	41.4/41.4	.114+.416σ	14	.131	1.149	1.11
3	33.55/33.55	.0716+.625σ .13	11 12			
	Average	.1008		.0981	.973	.934
3.5	31/31	.09	13	.0875	.972	972
5	25.8/25.8	.056+.54σ	11	.0672	1.200	1.048
7	21.8/21.8	.040+.55σ	11	.0525	1.312	1.089

The calculated values of steady-state drag coefficients for ogives are about 12 percent higher than the average experimental values. It is interesting to note that a cavitation number change of $\sigma = .015$ would reduce this difference by approximately half. Any small error in cavitation number would not significantly reduce the differences for the blunter shapes.

The scant experimental data available pertaining to the steady-state drag coefficients of paraboloids of revolution are compared to calculated values in Table 3.

TABLE 3

Comparison of Steady-State Drag Coefficient
for Paraboloids of Revolution

L/D	Experimental $C_{ds\,(max)}$ (Form)	Ref.	Calculated $C_{ds(max)}$ (Total)	$C_{ds(max)}$ (Form)	Cal./ Exp. Form
1	.125	15	.138	.130	1.040
3.33	.025	15	.0415	.0150	.600

Agreement is much better for the blunt paraboloid than for any of the blunt ogives. The discrepancy for the fine paraboloid may be due to the method used in reference (15) to adjust the experimental data to zero cavitation number. However, when the friction drag coefficient is added to the form drag coefficient to obtain the steady-state drag coefficient, the difference is less than 20 percent.

The principal purpose of this report is to propose a method for computing the total drag coefficient for pointed axisymmetric shapes during vertical water entry. In order to evaluate the accuracy of this technique, the total drag coefficient versus depth of penetration function was computed for all relevent shapes for which water-entry data was available. The results for cones have been previously discussed. The calculated values for ogives and cusps are graphically compared with the experimental data in Figures 4-7 and in Appendix C. The impact data for other shapes such as paraboloids were not found. However, current studies on such shapes should yield such data in the near future.

Numerical comparisons were easily possible with the four shapes reported in reference (8). The same instrumentation and type of models were used in this study as were used in the study of cones, which gave the basic emperical data for this method. Hence, if the method has any usefulness, one would expect good agreement between the calculated functions and the experimented results. The comparison of the values of maximum total drag coefficients and depth at which the drag coefficients become maximum are shown in Table 4.

It is seen that for cusps the calculated value for the maximum drag coefficient is about 12 percent higher than in the experimental results. This is somewhat greater than the error in reproducing the cone data. Perhaps the cusps have a larger percent roll-off than cones. The ogives are both computed about four percent low, which is interesting because the steady-state drag coefficients for these shapes were computed higher than the experimental values. In each of the four cases, the computed depth at which the maximum drag coefficient occurs agreed with the experimental data to within four percent. Figures 4, 5, 6 and 7 show the graphical comparison between the computed drag coefficients and the experimental results for these four shapes.

A comparison of computed maximum drag coefficients with experimental results for various tangent ogives is shown on Figure 8. The ogives reported in reference (8) were all secant ogives and were corrected to tangent ogives by the ratio of reference areas. As with the numerical comparison shown in Table 4, the computed values of the maximum total drag coefficients seem to be slightly lower than most of the experimental results. The sudden increase in computed drag coefficient values is caused by friction. This effect is accentuated because at a total cone angle of about 12 degrees and finer, the steady-state drag coefficient does not have a maximum value on the body. Hence, the friction drag is applied to the entire surface of the forebody. This result implies that the forebody becomes fully wetted for cone angles of 12 degrees and less. There has been no experimental verification of this prediction of wetting; therefore, the predicted drag values for very fine ogives should be used with care.

The graph of calculated maximum total drag coefficients for ogives and cusps with a 60-degree cone angle is shown on Figure 9. Also shown are the experimental values for four such shapes. As before, the calculated values for the cusp and cone are too large, while the calculated values for the ogives are probably too small.

13

TABLE 4

Comparison of Maximum Drag Coefficient
for Ogives and Cusps

Ogive	C_{dmax} Exp.	C_{dmax} Pred.	Pred. Exp.	Depth of C_{dmax} Exp.	Depth of C_{dmax} Pred.	Pred./exp.
60/43	.3027	.2806	.927	1.091	1.056	.968
88.4/321	.6854	.6516	.951	.978	.980	1.002
Cusp						
59.94/-43.4	1.481	1.658	1.120	2.286	2.268	.992
88.84/-31	2.366	2.670	1.128	1.295	1.281	.989

SUMMARY AND CONCLUSIONS

An empirical method of predicting the drag coefficient for vertical water entry of pointed shapes was developed. This method applied the experimental results previously obtained for the vertical water entry of cones of various angles to the geometric shape of the forebody of interest. Predicted drag coefficient functions agreed to within ±25 percent of the available experimental results. The computer program, written in BASIC, was used to calculate the predicted drag coefficient function; it is given in Appendix B. For those who wish to write their own program, the method of prediction consists of the following steps:

1. Determine an expression for the instantaneous transitory drag coefficient for all cone angles.

2. Determine an expression for the instantaneous forebody pressure drag coefficient for all cone angles.

3. Determine an expression for penetration ratio for all cone angles.

4. Define the zone of action to lie between the original water surface and the effective water surface.

5. Divide the forebody into computing stations beginning at the tip.

6. For each station, compute the effective surface position by adding the effect of penetration ratio for all stations to the tip.

7. Calculate the friction drag from the tip to the effective surface associated with each station, and convert to coefficient form.

8. Calculate the pressure drag coefficient based upon the angle of the forebody at each effective surface position.

9. Add the friction drag coefficient and the forebody pressure drag coefficient to obtain the steady-state drag coefficient.

10. Use the value of the first maximum of the steady-state drag coefficient for all stations at greater depths.

11. At each station, calculate the transitory drag coefficient, using the maximum body angle in the zone of action.

12. Add the steady-state drag to the transitory drag coefficient to obtain the total drag coefficient at each station.

13. At stations for which the forebody base has been wetted, reduce the transitory drag coefficient proportionally to the cone of the last calculation angle.

REFERENCES

1. Von Karman, "The Impact of Seaplane Floats During Landing", NACA TN 3211, 1929

2. Wagner, H., "Landing of Seaplanes", NACA TN 622, 1931

3. Mayo, W. L., "Analysis and Modification of Theory for Impact of Seaplanes on Water", NACA Report No. 810, 1945

4. Pierson, J. D., "On the Virtual Mass of Water Associated with an Immersing Wedge", Journal of the Aero. Sc., June 1951

5. Baldwin, J. L., "Vertical Water Entry of Cones", NOLTR 71-25

6. Weible, A., "The Penetration Resistance of Bodies with Various Head Forms at Perpendicular Impact on Water", German Avia. Res. Report No. 4541, Naval Research Transl. NRL Trans. No. 286, Revised (1952)

7. Shiffman, M. and Spencer, D. C., "The Force of Impact on a Cone Striking a Water Surface (Vertical Entry)", Comm. Pure and Appl. Math., Vol. IV (1951)

8. Baldwin, J. L., "Vertical Water Entry of Some Ogives, Cones, and Cusps", NSWC/WOL/TR 75-20

9. Hoerner, S. F., Fluid Dynamic Drag, 1965

10. Oversmith, R. H., "Some Observations on Cavitating Flows", Convair Engr. Dept., Rept. ZR-659-015 (1959)

11. Shaw, R. A., "Underwater Projectiles, Prediction of Underwater Behavior from Wind Tunnel Measurements", MAEE Helensburg Rept. H/ARM/RES23 (1944)

12. Birkhoff, G., Summary Tech Rep. of the Nat. Def. Res. Comm., "Mathematical Studies Relating to Military Physical Research", Vol. 1, 1946

13. Waugh, J. G. and Ager, R. W., "Water Entry Whip and Deceleration of Six Full-Scale Torpedo Models with Ogive and Plate-Ogive Heads", NAVORD Report 1308 NOTS 378, 1951

14. Eisenberg, P. and Pond, H. L., "Water Tunnel Investigations of Steady-State Cavities", DTMB Report 668 (1948)

15. Johnson, V. E. and Rasnick, T. A., "The Drag Coefficient of Parabolic Bodies of Revolution Operating at Zero-Cavitation Number and Zero Angle of Yaw", NACA TR R-86 (1960)
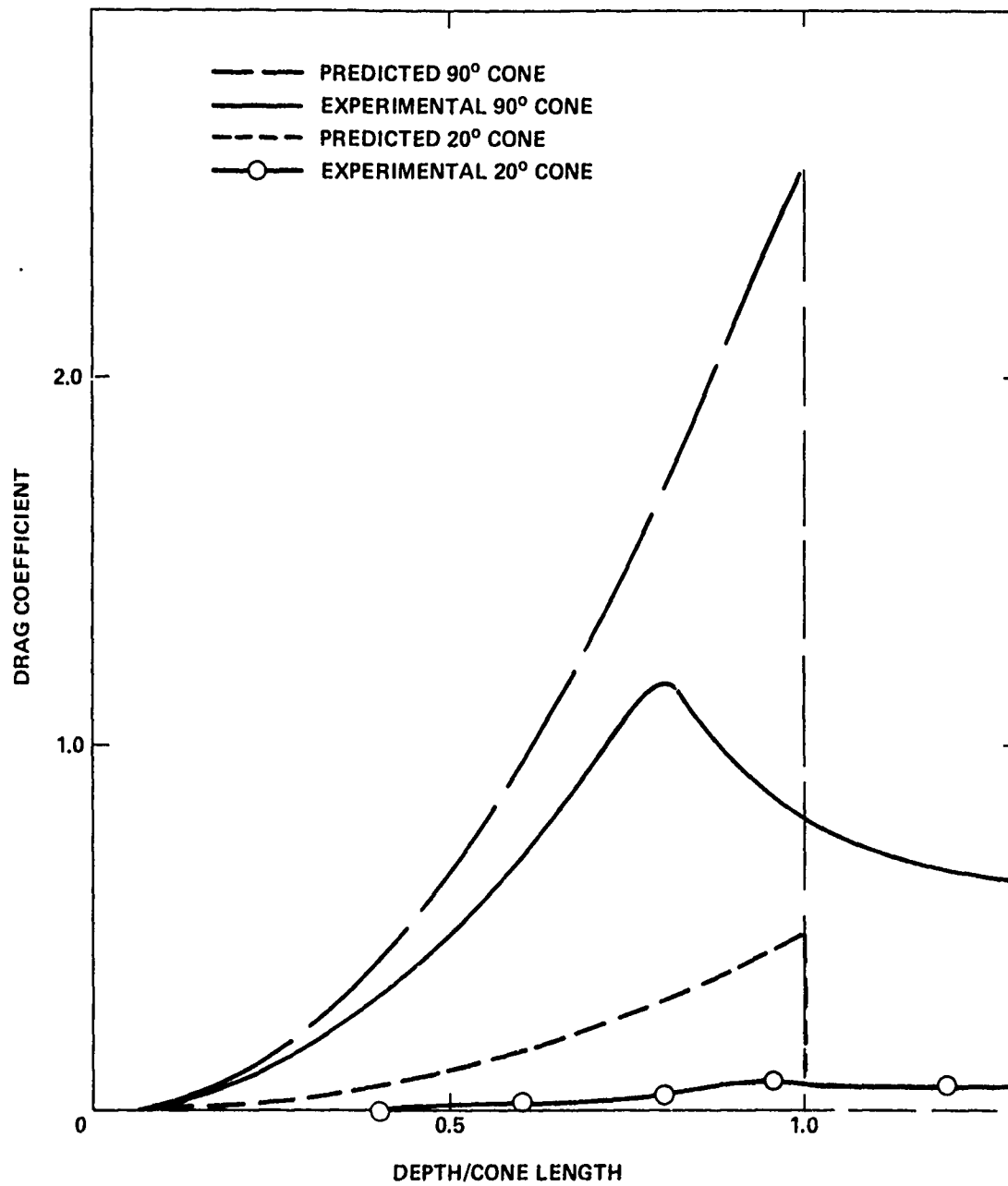
FIG. 1 EXPANDING DISK PREDICTIONS FOR 90 AND 20 DEGREE CONES
COMPARED TO EXPERIMENTAL RESULTS

18
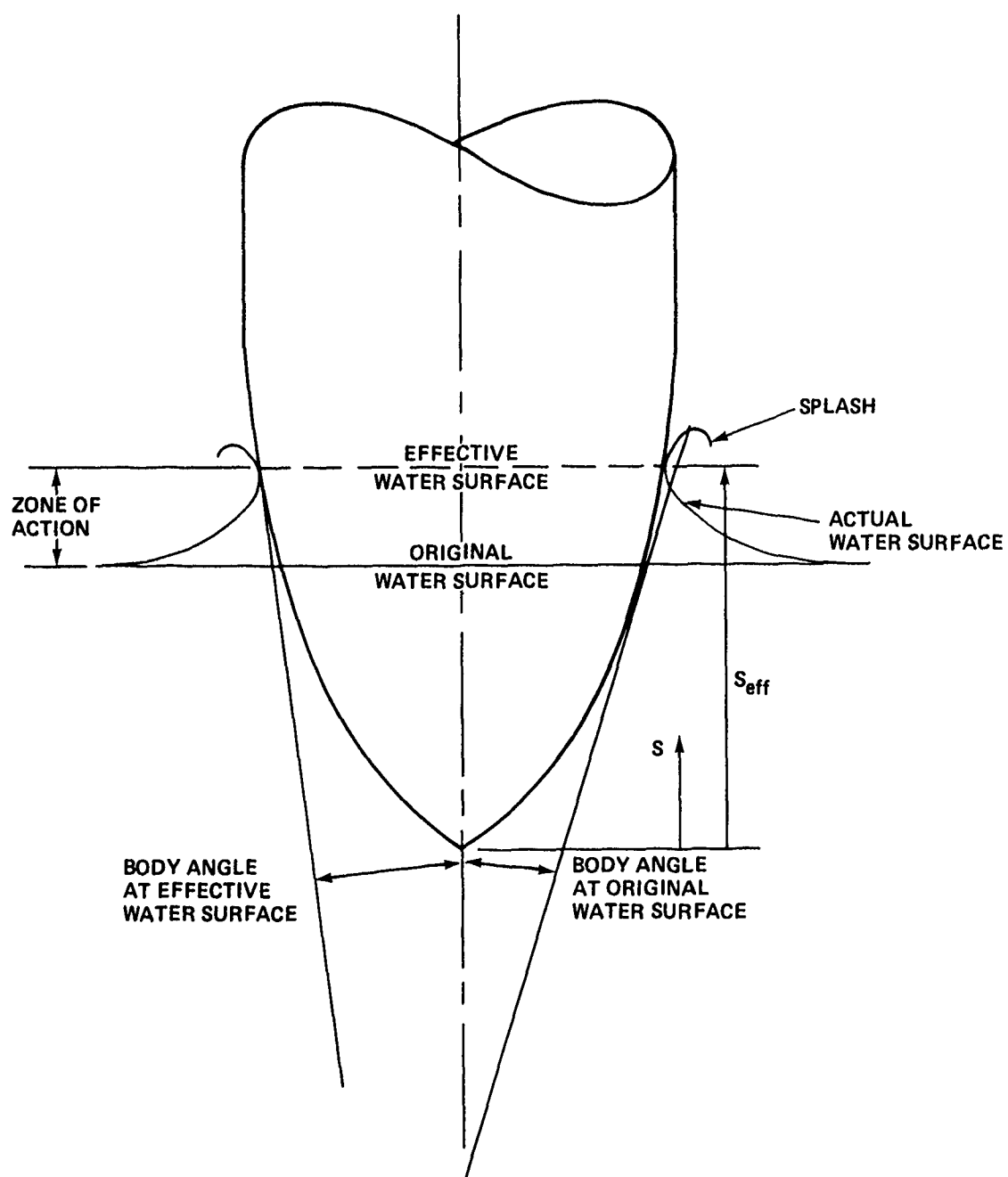
FIG. 2 WATER ENTRY NOMENCLATURE

19

ORIGINAL WATER SURFACE

EQUIVALENT CONE FOR STEADY STATE
PRESSURE DRAG COEFFICIENT AND
TRANSIENT DRAG COEFFICIENT FOR
CONVEX SHAPE

EFFECTIVE WATER SURFACE

EQUIVALENT CONE FOR TRANSIENT
DRAG COEFFICIENT FOR CONVEX SHAPE
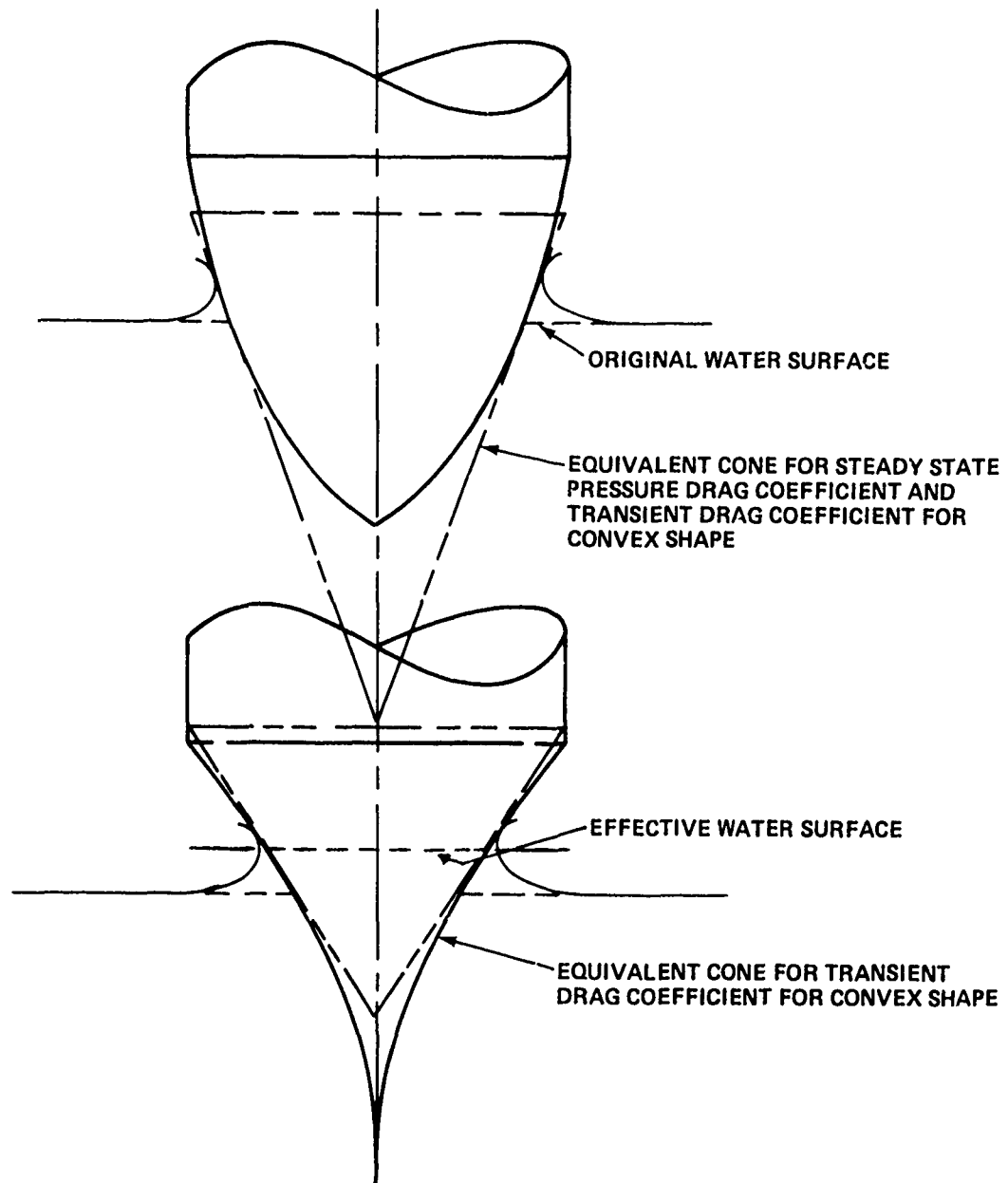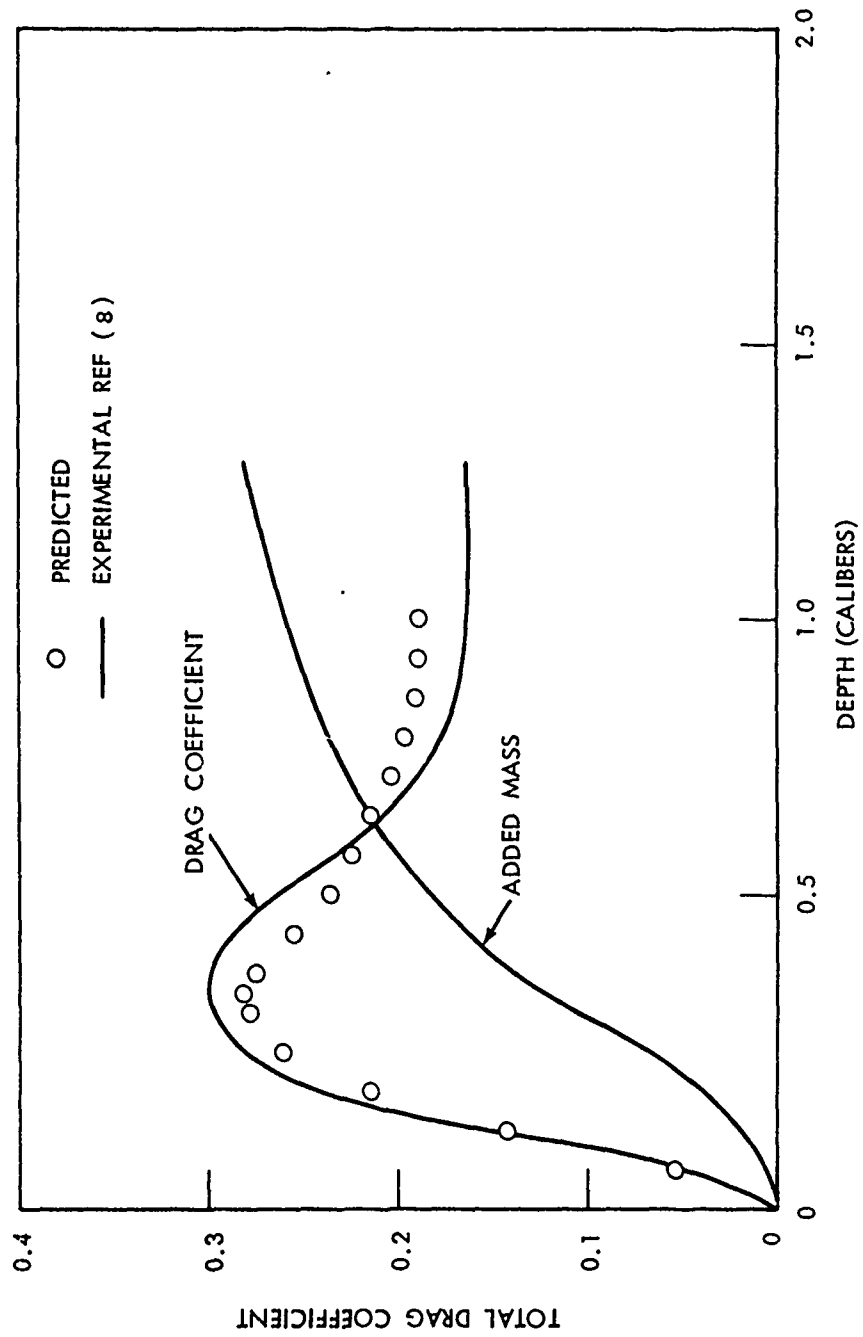
FIG. 3 EQUIVALENT CONES

20

FIG. 4 TOTAL DRAG COEFFICIENT VS DEPTH FOR 60/43 OGIVES
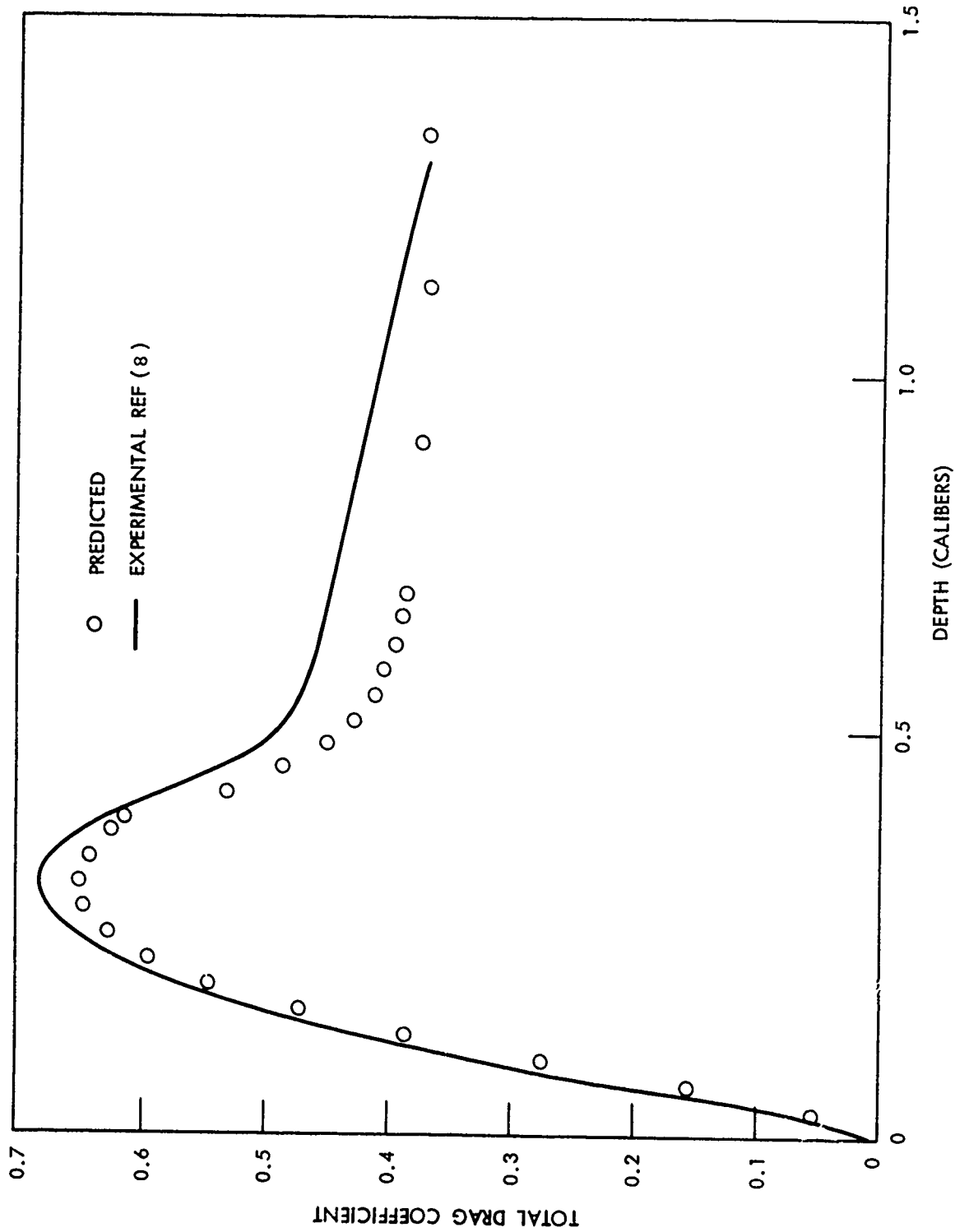
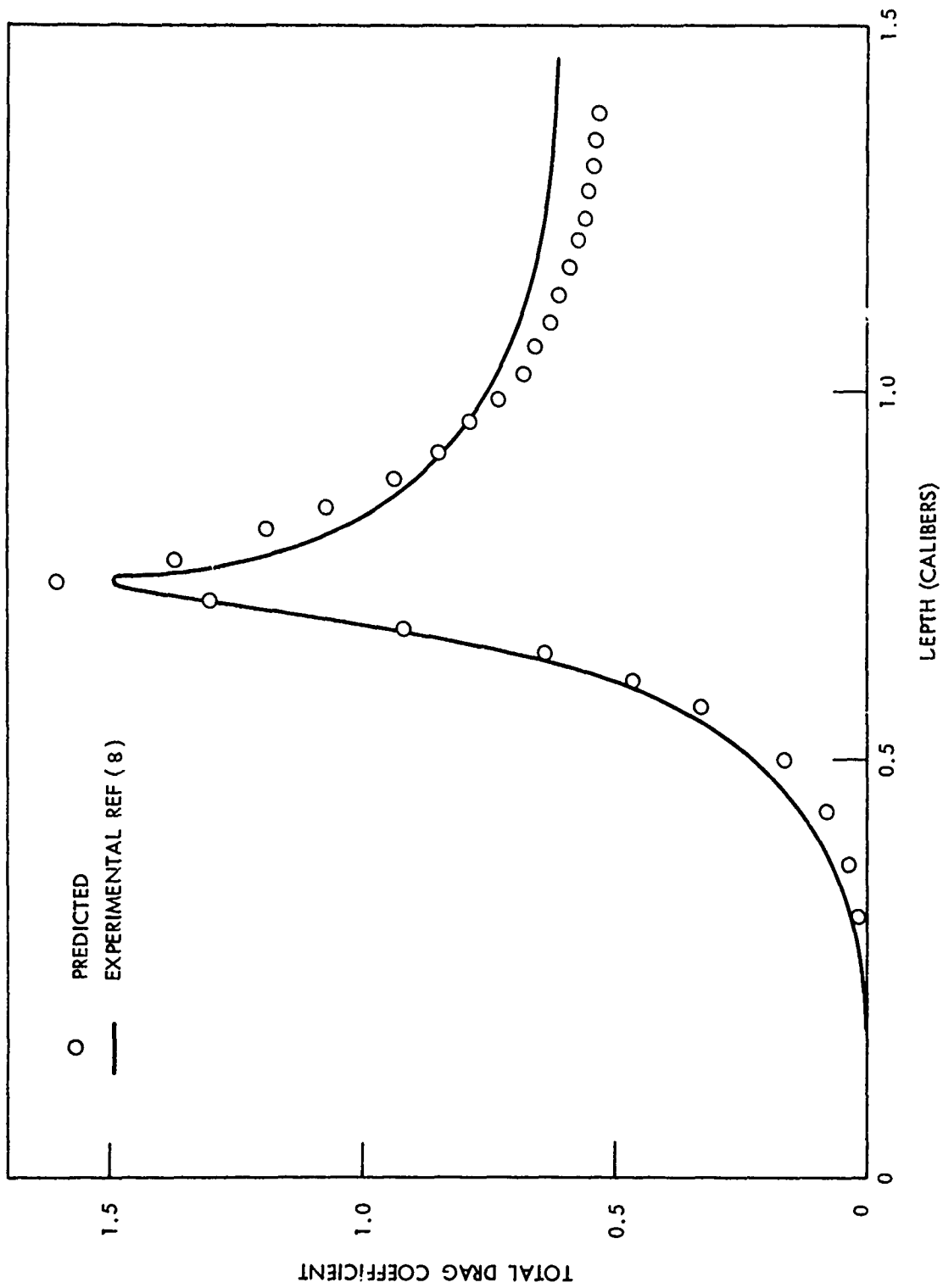FIG. 5 TOTAL DRAG COEFFICIENT VS DEPTH FOR 88.4/32 OGIVES

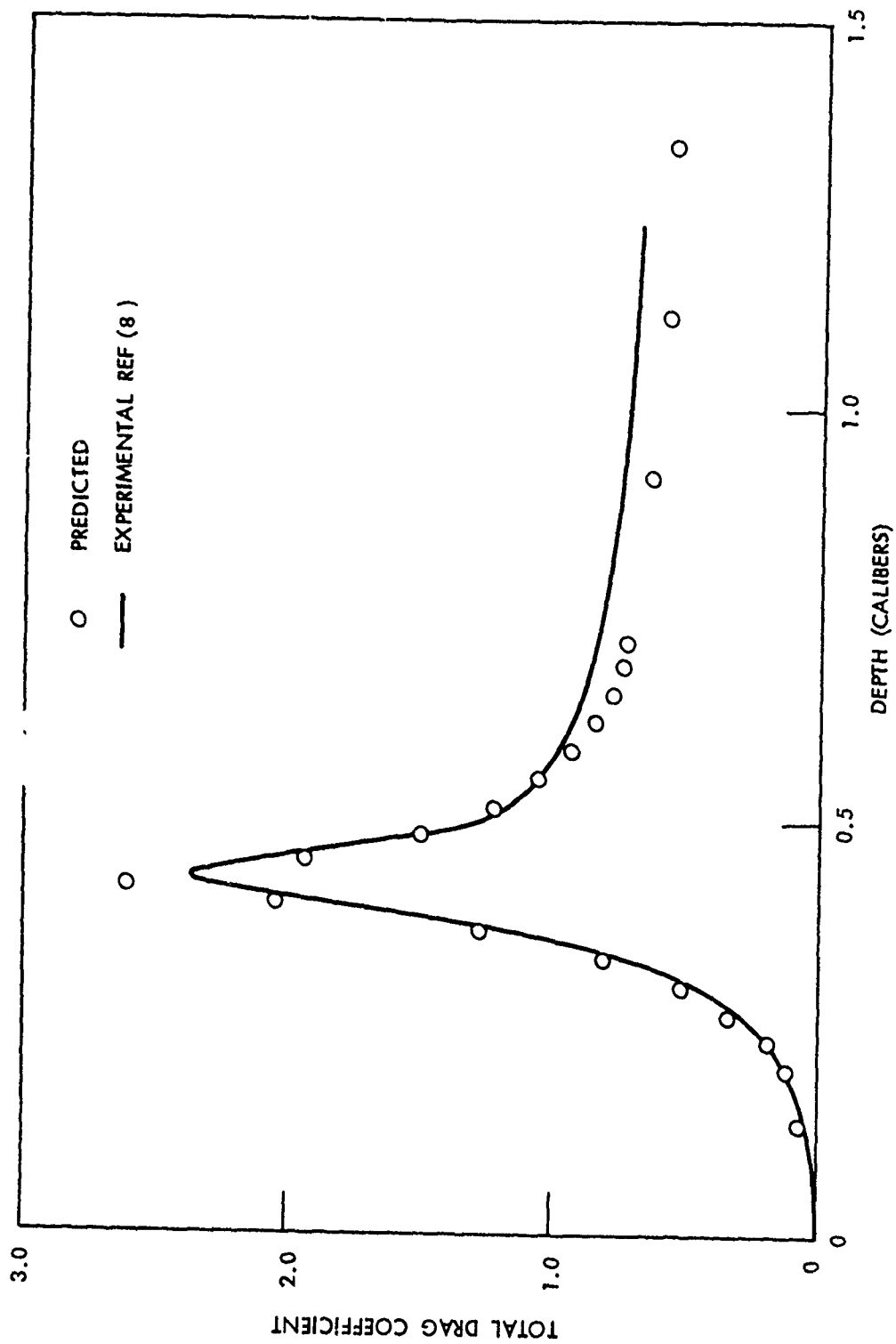FIG. 6 TOTAL DRAG COEFFICIENT VS DEPTH FOR 59.94/−43.4 CUSPS

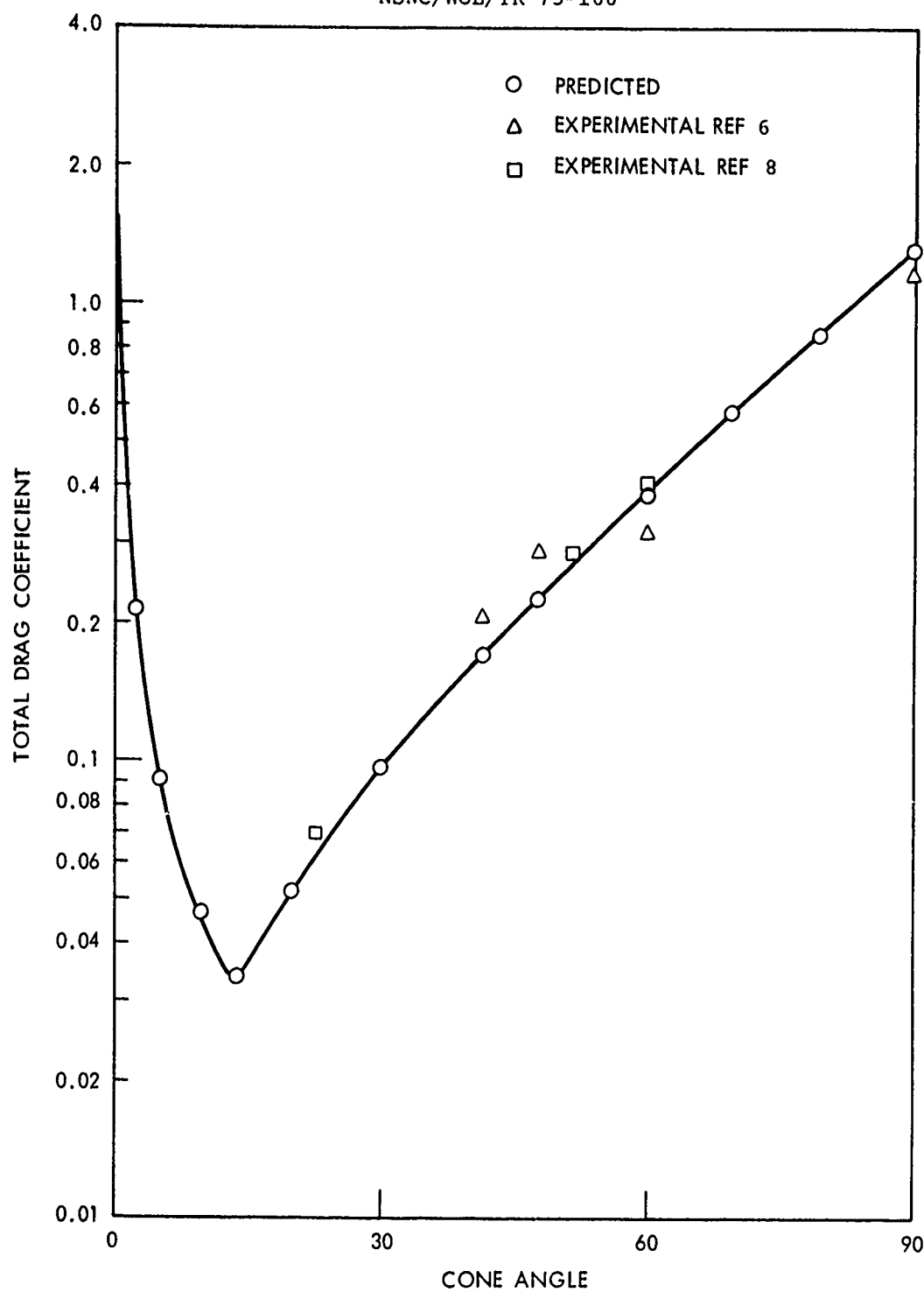23

FIG. 7 TOTAL DRAG COEFFICIENT VS DEPTH FOR 88.94/-31
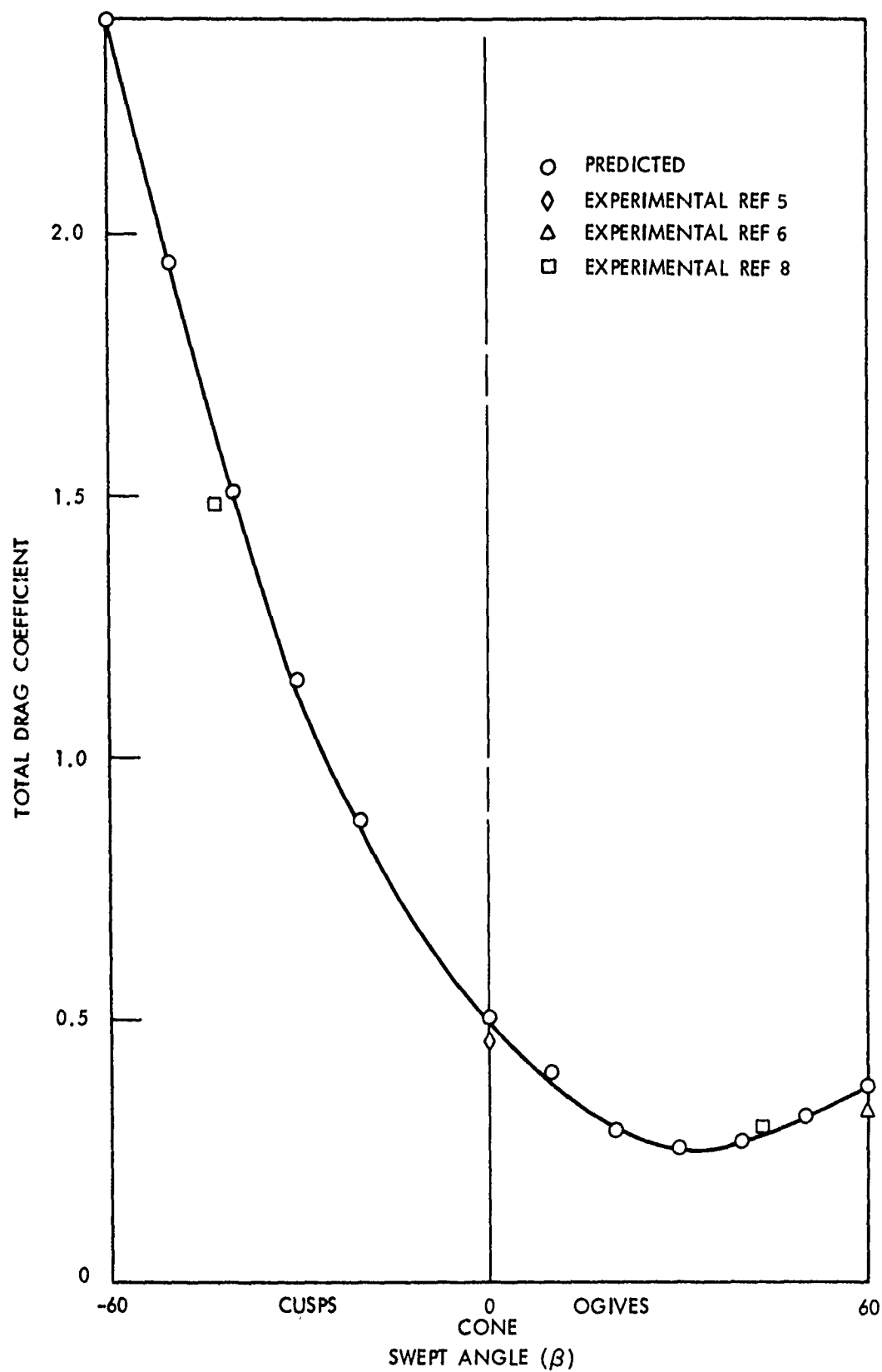
FIG. 8 TOTAL DRAG COEFFICIENT VS CONE ANGLE FOR
TANGENT OGIVES

25

FIG. 9 TOTAL DRAG COEFFICIENT VS SWEPT ANGLE FOR 60/β OGIVES

APPENDIX A

BASIC EQUATION

The equation relating the momentum just before first contact with the momentum at some later time is given as Equation (1), and the force equation is given as Equation (2)

$$U_o M - U(M+m) = \int_o^t B \, dt - Mgt + \frac{\rho}{2} \int_o^t C_{ds} A U^2 dt \qquad (1)$$

$$-\frac{dU}{dt}(M+m) - U\frac{dm}{dt} = B - Mg + \frac{\rho}{2} C_{ds} A U^2 \qquad (2)$$

Substituting $U^2 \frac{dm}{ds}$ for the second term of Equation (2) and rearranging terms gives:

$$-\frac{dU}{dt}(M+m) - B + Mg = \frac{dm}{ds} U^2 + \frac{\rho}{2} C_{ds} A U^2 \qquad (3)$$

If the total drag coefficient is defined as

$$C_d = \frac{2}{\rho A} \frac{dm}{ds} + C_{ds} \qquad (4)$$

then Equation (3) may be rewritten as

$$-\frac{dU}{dt}(M+m) - B + Mg = \frac{1}{2} \rho C_d A U^2 \qquad (5)$$

The value of added mass (m) and $\frac{dm}{ds}$ can be calculated using Equation (3) and the total drag coefficient C_d was computed from Equation (4). However, a simpler procedure is to determine m from (1) and C_d from (5). In order to ensure an accurate evaluation of the integrals in Equation (1), the added mass (m) was also computed by integrating $\frac{dm}{ds}$ as given in Equation (4) using the computed value of C_d.

For the vertical entry of cones, the added mass should be given by

$$m = \rho k r^3 = \rho k (\tan \frac{\phi}{2})^3 s^3 \qquad (6)$$

A-1

Then

$$\frac{dm}{ds} = 3\rho k \left(\tan \frac{\alpha}{2}\right)^3 s^2 \tag{7}$$

Substituting (7) into (3) yields

$$-\frac{dU}{dt}(M+m) - B + Mg = \left(3\rho k \left(\tan \frac{\alpha}{2}\right)^3 s^2 + \frac{\rho}{2} C_{ds}A\right)U^2 \tag{8}$$

If the total mass constant (K) is defined as:

$$K = k + \frac{C_{ds}}{6}\left(\tan \frac{\alpha}{2}\right)^{-1}\pi \tag{9}$$

then (8) can be rewritten as

$$-\frac{dU}{dt}(M+m) - B + Mg = 3\rho K \left(\tan \frac{\alpha}{2}\right)^3 s^2 U^2 \tag{10}$$

This form of the equation was chosen to compare easily the experimental results with the theoretical results obtained in reference 3.

It should be noted that the total mass constant (K) is also a drag coefficient related to the area intersected by the original water surface. The relationship between the mass constant (K) and the total drag coefficient C_d is obtained by subtracting Equation (5) from Equation (10) and dividing out ρ and U^2:

$$C_d = 6K\left(\tan \frac{\alpha}{2}\right)^3 s^2 (A)^{-1} \tag{11}$$

If the area used to relate C_d to drag force is the area intersected by the heaved water surface, then the instantaneous drag coefficient is given by

$$C_{d_i} = \left(6K \tan \frac{\alpha}{2}\right)(\pi)^{-1} \tag{12}$$

A-2

OGIVE GEOMETRY

There seems to be no standard method used in the literature to define ogive shapes. An ogive shape is a pointed body formed by rotating a circular arc. If the water-impact forces do indeed depend chiefly upon the geometry of the body, the shape will have to be defined more precisely. The method chosen for use in this report uses two angles and one reference length. One angle is the tip angle of a cone of the same length and base as the ogive and the other angle is the arc length (swept angle) used to generate the ogive section. The base diameter is used as the reference length. The tip angle, base angle, slopes, and radii are all easily computed for both normal ogives and inverse ogives (cusps), as shown in Figure A-1. Note that in Figure A-1 the inclusion of a minus sign with the swept angle β changes the ogive to the cusp. An inspection of the computer program shows a continuing similarity in the geometric equations. The only difference, if any, is a minus sign for the cusp shape. The swept radius r is one parameter that has the same equation for both shapes.

$$r = r/2 \sin (\alpha/2) \sin (\beta/2)$$

In the comparison of the results for different ogives, it is often possible to relate the forces to the base area of a tangent ogive. A method for computing the ratio between the base area of a secant ogive and corresponding tangent ogive is shown in Figure A-2. Also, the nomenclature must be such that the actual tip angle remains constant.

In this report it is assumed that the tangent ogive is a limit of this geometric family of shapes. This implies that the swept angle may not be larger than the cone angle. It is also defined that the limit case for cusps is when the swept angle is equal to the cone angle. For cone angles of 90 degrees or more, this definition merely states that the base angle cannot be negative.

A-3
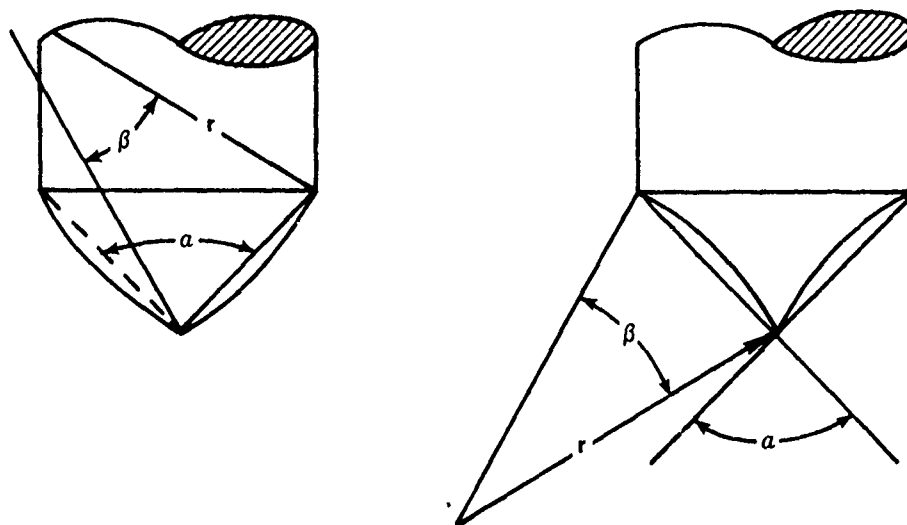
OGIVE	PROPERTY	CUSP
a/β	"NAME"	$a/-\beta$
$a + \beta$	TIP ANGLE	$a - \beta$
$a - \beta$	BASE ANGLE	$a + \beta$

FIG. A-1 OGIVE GEOMETRY

A-4
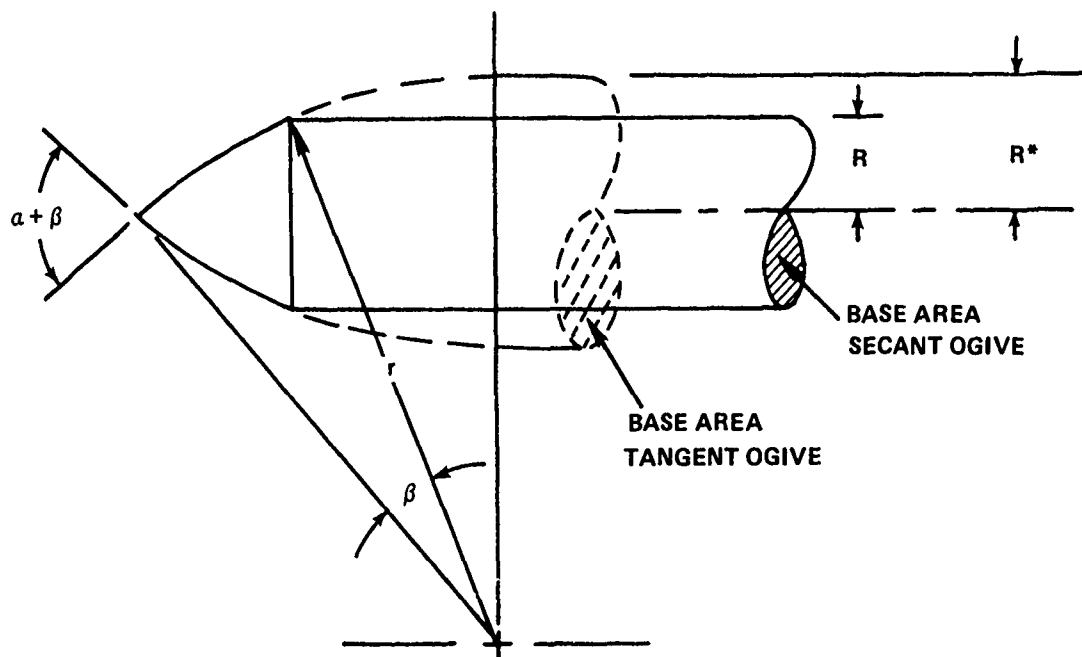
BASE AREA RATIO = $(R/R^*)^2$

$$(R/R^*)^2 = \left(\frac{2\sin a/2 \, \sin\beta/2}{1 - \cos\frac{a+\beta}{2}}\right)^2$$

FIG. A-2 BASE AREA COMPARISON OF SECANT AND TANGENT OGIVES

A-5

APPENDIX B

This section consists of a listing and sample run of the computer program written in BASIC used to calculate the predicted values of the drag coefficient given in this report. By the selection of suitable constants, it is possible to obtain predicted drag coefficient versus depth functions for shapes defined by the polynomial

$$R = K1*D + K2*D^2 + K3*D^3 + K4*D^4 + K5*D^5 + K6*D^{.3}$$

or for ogives or cusps. It is also possible to obtain the printout either at the point of the first maximum of the total drag coefficient or at uniformly spaced distance intervals. The format used in this program was chosen in an effort to allow ready understanding, easy modification, and maximum flexibility.

The major sections of the program are:

Lines 100-180 consist of an alphabetical list of constants needed to operate the program.

Lines 200-550 contain the commands that establish the order of calculations. Also the penetration ratio is calculated on line 250.

Line 554 contains the print command used with the condensed print format.

Lines 700-790 contain the calculation of the radius and angle for shapes defined by the polynomial.

Lines 900-990 contain the calculation of the radius and angle for ogives and cusps. The headings used with these shapes are also printed.

Lines 1200-1290 contain the calculations of the skin friction drag coefficient. A constant value of .003 is assumed for the friction drag coefficient.

Lines 1400-1490 contain the calculations of steady-state pressure drag coefficient.

Lines 1600-1690 contain the calculations of the transitory drag coefficient.

Lines 2000-2290 contain the calculations of transitory and total drag coefficients provided the base of the forebody shape is submerged.

Lines 8000-8100 contain the print statements used with the long print format.

In order to run a problem it is necessary to enter the following constants. Note: all distances must have the same units and determine the unit used in output.

1. Line 115 D1 = distance between computational step.
                In long print format every tenth
                computational step is printed

2. Lines 135-151 K1-K6 = coefficients of polynomial
    Lines 152 K1 = total cone angle in degrees of ogive or cusp
    Lines 153 K8 = swept angle in degrees of ogive or cusp

3. Lines 154 P = -1 for cusp
             P = 1 for ogive
             P = 2 for polynomial

4. Line 157 P4 = 0 printout of first maximum only
             P4 = 1 full printout

5. Line 160 R 1 = radius of base

The various constants are defined as:

A.   temporary name for an angle
A.   body angle at the original water surface
A3   previous A4

A4   body angle at the effective surface

C   C6 when R4=R1
C1   incremental friction drag coefficient
C2   friction drag coefficient
C3   previous C4
C4   steady-state pressure drag coefficient
C5   previous C6
C6   transitory drag coefficient
C7   previous C8
C8   total drag coefficient (C2 + C4 + C6)

D1   distance increment
D2   distance from tip to original water surface
D3   D1/H
D4   distance from tip to effective water surface

H   penetration ratio

K1-K6   constants that determine the polynomially defined
        shapes

K7   cone angle of ogive or cusp

K8   swept angle of ogive or cusp

M2   distance from tip to base for ogive or cusp

P   shape control (input on line 154)
P1   print control full printout only
P3   heading control (heading printed once only)
P4   print control (input on line 157)
P5   control that stops for first maximum

Q   radius of curvature of ogive or cusp

R1   base radius
R2   body radius at original water surface
R3   previous P4
R4   body radius at effective water surface

S   temporary area
S1   base area
S2   cross section area at original water surface
S4   cross section area at effective water surface
S6   surface area increment

Z   dummy

LIST   Fig. B-1 - Listing and Sample Run of Computer
                     Program Written in BASIC

75/07/10. 17.19.18.
PRØGRAM   ØBJ464

```
101     LET A4=.0001
102     LET C2=0
105     LET C4=0
110     LET C8=0
115     LET D1=.01
120     LET D2=0
125     LET D4=0
130     LET D5=0
134     LET K=1
135     LET K1=0
140     LET K2=0
145     LET K3=0
149     LET K4=0
150     LET K5=.38
151     LET K6=0
152     LET K7=60
153     LET K8=43
154     LET P=1
155     LET P1=-1
156     LET P3=1
157     LET P4=2
158     LET P5=0
160     LET R1=1
165     LET R3=0
166     LET R4=0
170     LET S1=3.14159*R1↑2
180     LET Z=0
200     LET P1=P1+1
209     IF P4=0 THEN 220
210     IF P1<9.5 THEN220
215     GØ SUB 8000
220     LET D2=D2+D1
230     LET D=D2
235     IF P<1.5 THEN 245
240     GØ SUB 700
241     REM SUB 900 IS FØR ØGIVES
243     GØ TØ 250
245     GØ SUB 900
250     LET H=1-.6905E-2*A+8.745E-5*A↑2-6.567E-7*A↑3
260     LET A2=A
270     LET R2=R
280     LET D3=D1/H
290     LET D4=D4+D3
300     LET D=D4
310     LET R3=R4
320     LET A3=A4
325     IF P<1.5 THEN 335
330     GØ SUB 700
```

CONT.

```
332     G0 T0 340
335     G0 SUB 900
340     LET A4=A
350     LET R4=R
360     IF  R4>R1  THEN 2000
370     IF  A4<.1  THEN 2000
380     G0 SUB 1200
385     G0 SUB 1400
390     IF  A4>A2  THEN  420
400     LET A=A2
410     G0 T0  450
420     LET A=A4
450     G0 SUB 1600
460     IF  P5>.5  THEN  470
461     LET C5=C2+C4
462 IF C3>C5 THEN 465
463     LET C3=C5
464     G0 T0  470
465     LET P5=1
470     LET C7=C8
480     LET C8=C3+C6
490     IF  C8<.02  THEN 200
500     G0 T0 510
510     IF C3<C4 THEN 530
520     LET C4=C3
530     LET C8=C3+C6
535     IF P4=0 THEN 540
536     G0 T0 550
540     IF  C7<C8 THEN 550
544     PRINT D2,C8,C3,A2,D4
546     G0 T0 9999
550     G0 T0 200
700     LET R=K1*D+K2*D↑2+K3*D↑3+K4*D↑4
705     LET R=R+K5*D↑.5+K6*D↑.3
710     LET A=K1+2*K2*D+3*K3*D↑2+4*K4*D↑3
715     LET A=A+.5*K5*D↑(-.5)+.3*K6*D↑(-.7)
720     LET A=57.3*ATN(A)
760     IF P3>1 THEN 790
762     PRINT "SHAPE GIVEN BY P0LYN0MIAL"
763     PRINT "P0LY C0NST ="K1,K2,K3
764     PRINT K4,K5,K6
765     PRINT
766     PRINT "B0DY RADIUS="R1
767     PRINT
768     PRINT "DIST","T0TAL CD","CDS","ANGLE","EFF DIST"
785     LET P3=2
790     RETURN
900     IF  P3=1 THEN 930
905     LET U=.5*K7/57.3
910     LET V=.5*K8/57.3
920     LET Q=R1/(C0S(U-V)-C0S(U+V))
930     LET X=Q*SIN(U+P*V)-P*D
```

CONT.

```
940     LET Y=SQR(G↑2-X↑2)
950     LET A=ATN(X/Y)
960     LET R=P*Q*(COS(A)-COS(U+P*V))
970     LET A=57.3*A
971     IF P3>1 THEN 990
972     IF P>-.5 THEN 975
973     PRINT"THE SHAPE IS A CUSP"
974     GO TO 976
975     PRINT "THE SHAPE IS AN OGIVE"
976     PRINT
977     PRINT "BODY RADIUS="R1
978     PRINT "CONE ANGLE ="K7
979     PRINT "SWEPT ANGLE ="K8
980     PRINT "RAD OF CURV ="Q
981     PRINT
982     PRINT"DIST","TOTAL CD","CDS","ANGLE","EFF DIST"
988     LET P3=2
990     RETURN
1200    LET S6=3.14159*(R3+R4)*D3
1210    LET C1=.003*S6/S1
1220    LET C2=C2+C1
1290    RETURN
1400    LET C3=C4
1410    LET C4=3E-3-1.36E-3*A+1.076E-3*A↑2-3.04E-5*A↑3+3.415E-7*A↑4
1420    LET C4=C4-1.362E-9*A↑5
1430    LET S=3.14159*R2↑2
1440    LET C4=C4*S/S1
1450    LET C4=C4/H↑2
1490    LET C9=C4
1600    LET C6=1.76E-2+1.093E-2*A-8.663E-4*A↑2+3.912E-5*A↑3
1610    LET C6=C6-2.556E-7*A↑4
1620    LET C6=C6*TAN((A-3)/57.3)
1630    LET C6=C6*S/S1
1690    RETURN
2000    PRINT
2005    LET D2=D2-D1
2010    GO SUB 8000
2015    IF P4<.5 THEN 9000
2020    LET A=A2
2030    IF P>.5 THEN 2050
2040    LET A=A4
2050    LET R=R1
2060    LET C=C6
2065    LET D=D2
2067    LET T9=A/57.3
2068    LET T8=TAN(T9)
2070    LET M2=D2
2080    LET T2=10*D1
2200    LET B4=.661*T2/M2
2210    LET A9=.3/(1+(T2/R1))↑2+EXP(-9*B4)
2220    LET S6=C*(1/1.3)*A9
2230    LET C8=C3+S6
2240    LET D2=T2+D
```

B-6

CONT.

```
2250    PRINT D2,C8
2260    LET T2=T2+10*D1
2262    IF T2<.8*D THEN 2270
2265    LET T2=T2+50*D1
2270    IF S6<.02*C3 THEN 9000
2290    GO TO 2200
2990    GO TO 9000
8000    PRINT D2,C8,C3,A2,D4
8050    LET P1=0
8060    LET Z=Z+1
8065    IF Z<4.5 THEN 8100
8070    PRINT
8075    LET Z=0
8100    RETURN
9000    LET Z=Z
9999    END
READY.
```

```
BYE

464        LOG OFF.   17.26.52.
464        CP         1.518 SEC.
```

RUN

75/07/10. 17.16.26.
PROGRAM 0BJ464

THE SHAPE IS AN OGIVE

BODY RADIUS= 1
CONE ANGLE = 60
SWEPT ANGLE = 43
RAD OF CURV = 2.72888

DIST	TOTAL CD	CDS	ANGLE	EFF DIST
.1	3.33095E-2	1.15109E-2	48.2419	.126227
.2	9.71428E-2	.038293	45.1794	.250941
.3	.161628	7.17684E-2	42.2736	.37427
.4	.214612	.106033	39.4961	.496305
.5	.252057	.136926	36.8255	.617108
.6	.273642	.161581	34.245	.736721
.7	.280685	.178187	31.7414	.855173
.8	.275171	.185841	29.3037	.972478
.9	.261225	.186357	26.9229	1.08864
1.	.247124	.186357	24.5914	1.20366
1.1	.234417	.186357	22.3025	1.31754
1.2	.223612	.186357	20.0506	1.43025
1.3	.21481	.186357	17.8305	1.54178
1.4	.207832	.186357	15.6378	1.6521
1.47	.203852	.186357	13.9005	1.73949
1.57	.198672			
1.67	.195151			
1.77	.192743			
1.87	.191084			
1.97	.189931			

CP 1.099 SECS.

RUN COMPLETE.

APPENDIX C

This section consists of graphs which compare the experimental and predicted values of total drag coefficient.
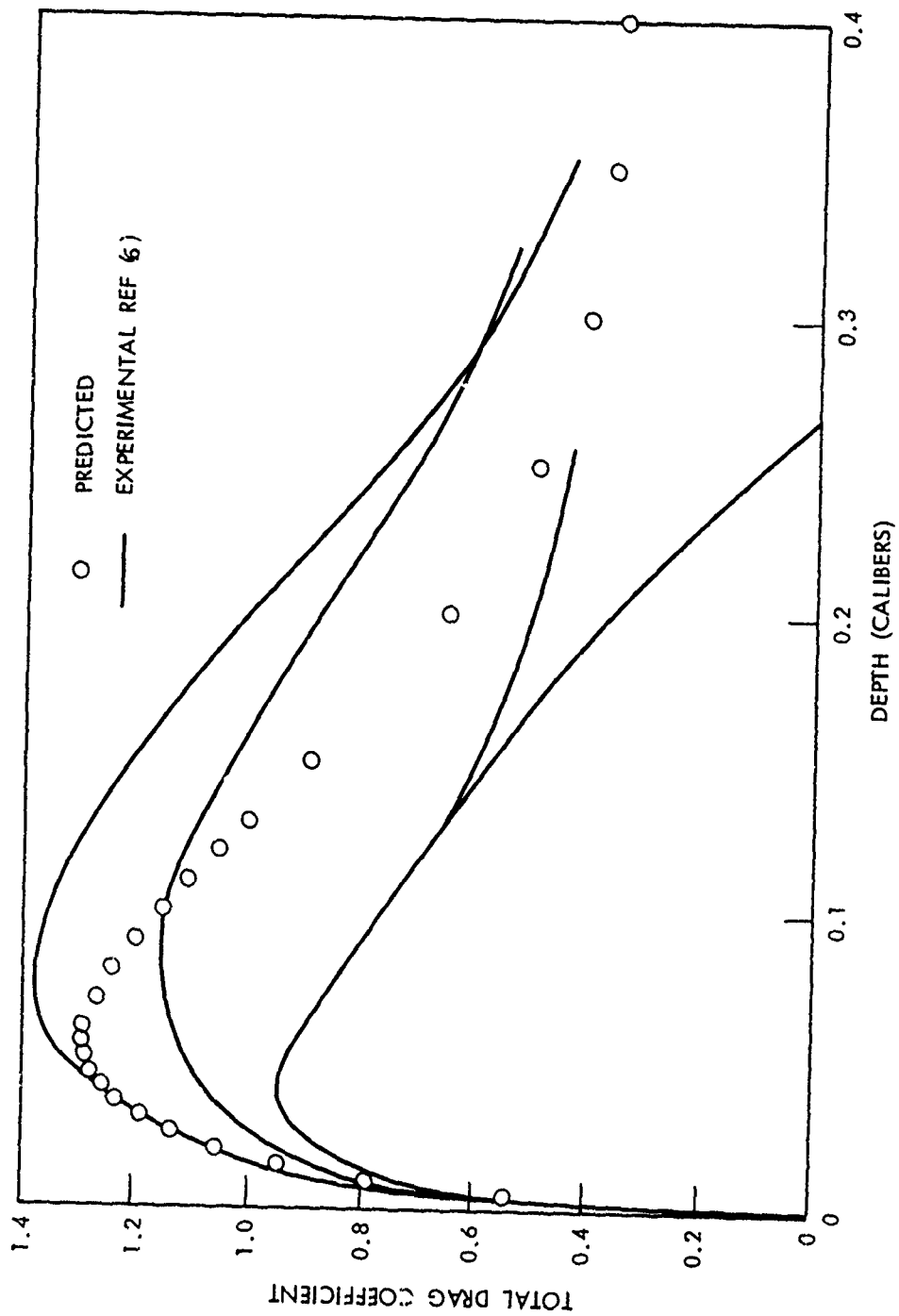
FIG. C-1 TOTAL DRAG COEFFICIENT VS DEPTH FOR 90/90 OGIVES (HEMISPHERES)
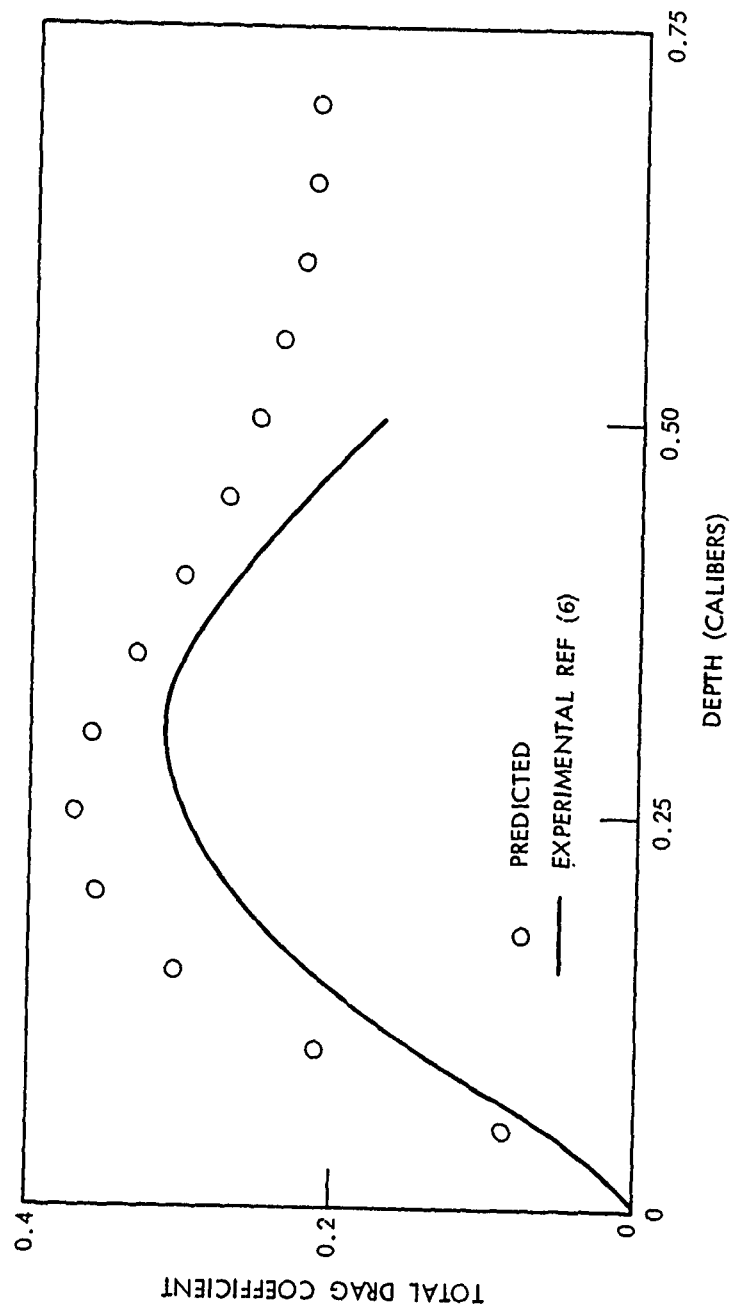
FIG. C-2 TOTAL DRAG COEFFICIENT VS DEPTH FOR 60/60 OGIVES
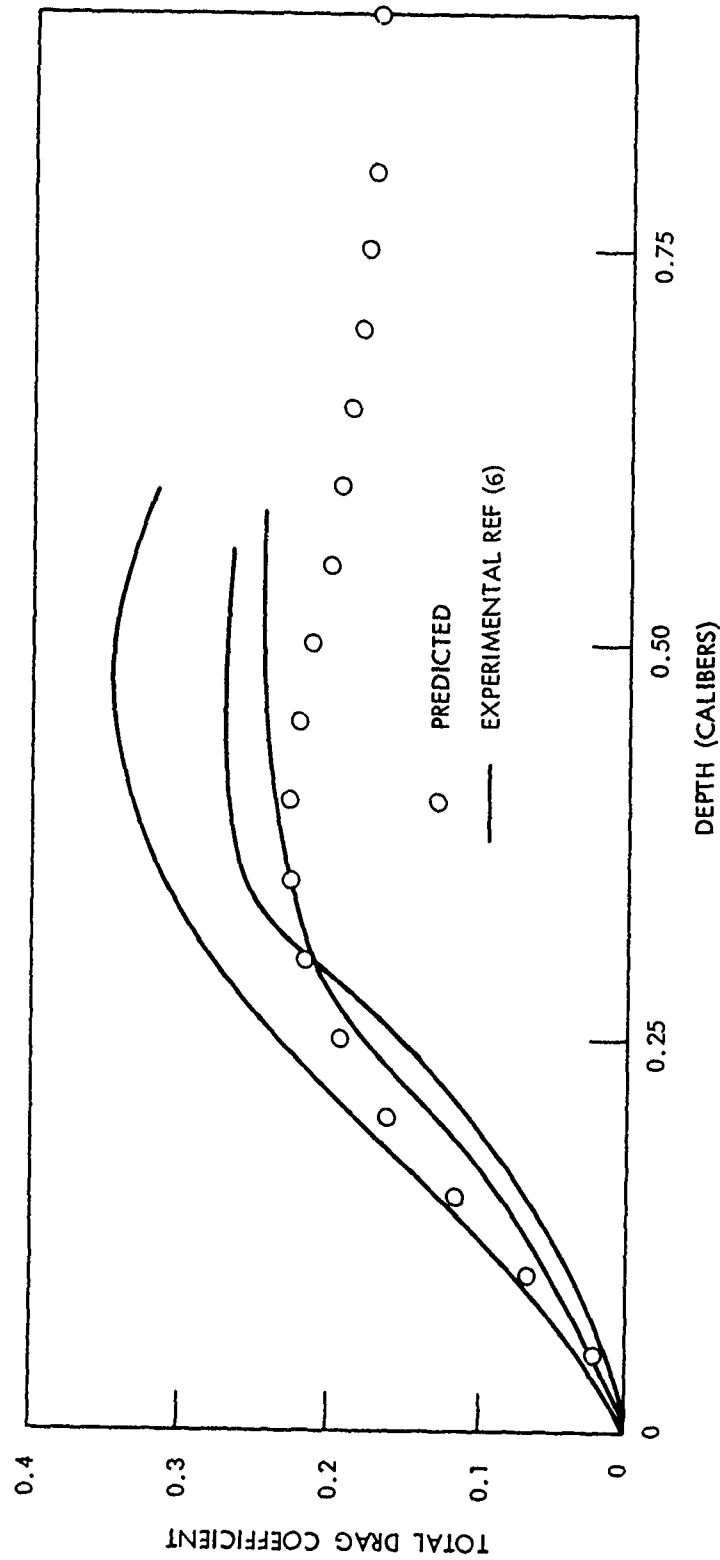
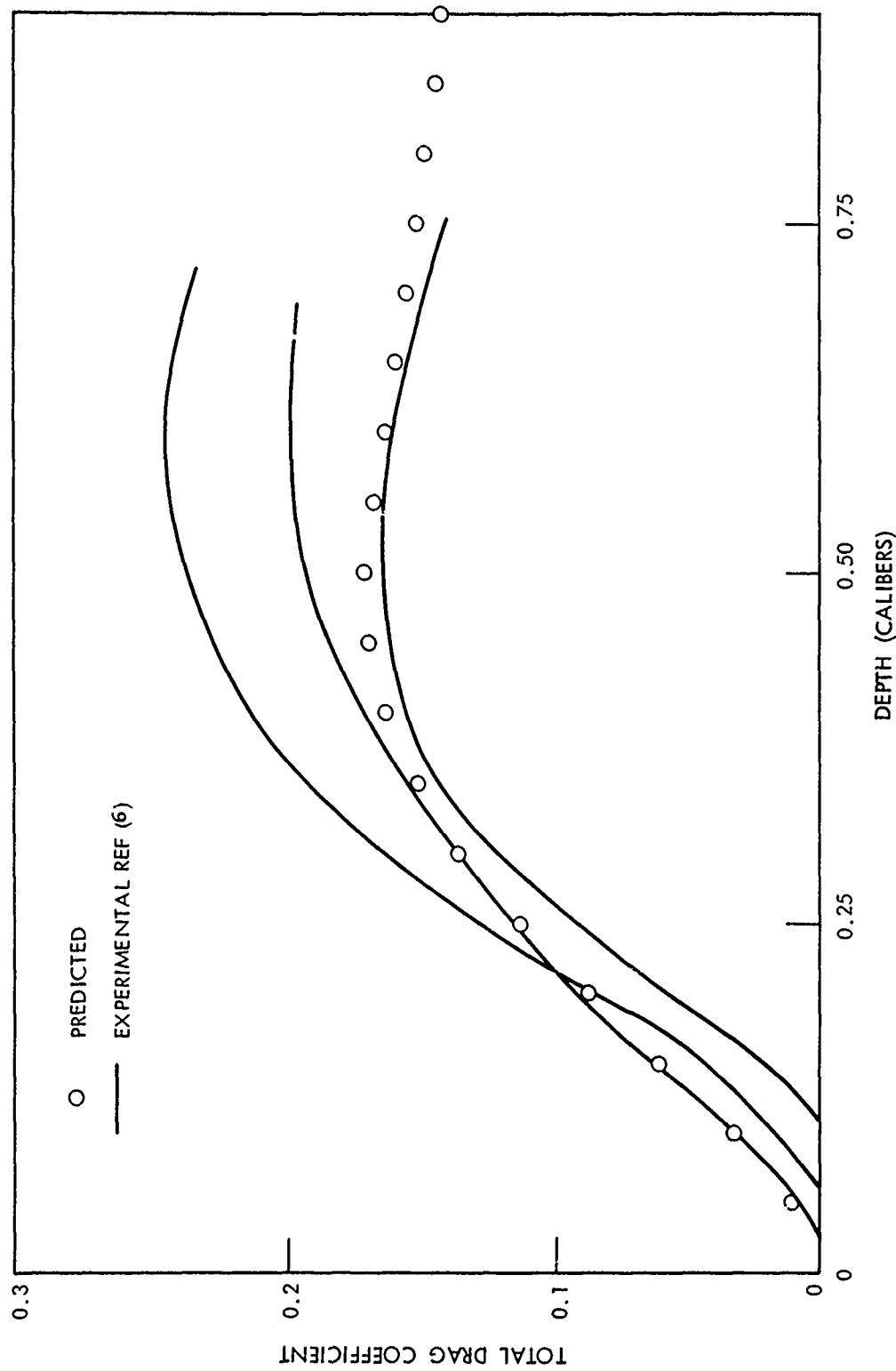FIG. C-3 TOTAL DRAG COEFFICIENT VS DEPTH FOR 48.18/48.18 OGIVES

FIG. C-4 TOTAL DRAG COEFFICIENT VS DEPTH FOR 41.44/41.44 OGIVES

DISTRIBUTION

Copies

Commander
Naval Air Systems Command
Washington, D. C. 20362
  Attn: AIR-530133A
         AIR-53712A
         AIR-350D
         AIR-35⌐
         AIR-350B
         AIR-030

Commander
Naval Sea Systems Command
Department of the Navy
Washington, D. C. 20362
  Attn: SEA-09G32   2
         SEA-03
         SEA-0351
         SEA-0372
         SEA-054
         SEA-05121
         PMS-0647

Office of Naval Research
Department of the Navy
Arlington, Virginia 22217
  Attn: ONR-438
         ONR-439
         ONR-463

Director
Defense Research and Engineering
The Pentagon
Washington, D. C. 20301

Defense Documentation Center
Cameron Station
Alexandria, Virginia 22314   12

Director of Research
National Aeronautics and Space Administration
600 Independence Avenue Southwest
Washington, D. C. 20546

1

Copies

NASA Scientific and Technical Information Facility
Post Office Box 33
College Park, Maryland   20740   2

Superintendent
U.S. Naval Postgraduate School
Monterey, California   93940
  Attn: Library

Commanding Officer
U.S. Naval Air Development Center
Warminster, Pennsylvania   18974
  Attn: NADC Library

Director
U.S. Naval Research Laboratory
Washington, D.C.   20390
  Attn: Library   2

Commanding Officer
Naval Ship Research and Development Center
Bethesda, Maryland   20084
  Attn: Code 154
          Code 1541
          Code 1556
          Code 5613

Commander
Naval Undersea Center
San Diego, California   92132
  Attn: Dr. A. Fabula
         Dr. J. Hoyt

Commanding Officer
Naval Underwater Systems Center
Newport, Rhode Island   02840
  Attn: J. F. Brady
         W. A. McNally
         R. H. Nadolink

Commander
Naval Weapons Center
China Lake, California   93555
  Attn: Library   2

2

Copies

Harry Diamond Laboratories
Washington, D. C. 20438
    Attn: Harry Davis
           Library

U.S. Army Ballistic Research Laboratories
Aberdeen Proving Ground, Maryland 21105
    Attn: Library

National Aeronautics and Space Administration
George C. Marshall Space Flight Center
Huntsville, Alabama 35812
    Attn: Library

National Aeronautics and Space Administration
Langley Research Center
Langley Station
Hampton, Virginia 23365
    Attn: Library

National Aeronautics and Space Administration
Lewis Research Center
21000 Brookpark Road
Cleveland, Ohio 44135
    Attn: Library

Director
Alden Research Laboratories
Worcester Polytechnic Institute
Holden, Massachusetts 01520   2

Applied Physics Laboratory
The Johns Hopkins University
Johns Hopkins Road
Laurel, Maryland 20810
    Attn: Document Librarian   2

Applied Research Laboratory
The Pennsylvania State University
Post Office Box 30
State College, Pennsylvania 16801
    Attn: Dr. Blaine R. Parkin
           Dr. J. W. Holl

AVCO Everett Research Laboratory
2385 Revere Beach Parkway
Everett, Massachusetts 02149
    Attn: Library

Copies

Battelle Memorial Institute
505 King Avenue
Columbus, Ohio 43201
  Attn: Library

The Boeing Company Aerospace Library
Post Office Box 3999
Seattle, Washington 98124

Garfield Thomas Water Tunnel Library
The Pennsylvania State University
Institute for Science and Engineering
Applied Research Laboratory
Post Office Box 30
State College, Pennsylvania 16801

General Electric Company
Post Office Box 8555
Philadelphia, Pennsylvania 19101
  Attn: MSD Library

Hydronautics, Incorporated
Pindell School Road
Laurel, Maryland 20810
  Attn: Mr. Philip Eisenburg   2

Iowa Institute of Hydraulic Research
State University of Iowa
Iowa City, Iowa 52240
  Attn: Dr. J. F. Kennedy   2

Jet Propulsion Laboratory
4800 Oak Grove Drive
Pasadena, California 91103
  Attn: Library

Lockheed Missiles and Space Company
Department 57-24, Building 150
P. O. Box 504
Sunnyvale, California 94088
  Attn: Robert Waid   2

Los Alamos Scientific Laboratory
Post Office Box 1663
Los Alamos, New Mexico 87544
  Attn: Report Library

4

Copies

Sandia Laboratories
Albuquerque, New Mexico 87115
  Attn: Mr. A. Stephenson
        Library

Director
Southwest Research Institute
Department of Mechanical Sciences
San Antonio, Texas 78206
  Attn: Library

Director
Saint Anthony Falls Hydraulic Laboratories
University of Minnesota
Minneapolis, Minnesota 55455
  Attn: Prof. E. Silberman

The Catholic University of America
Washington, D. C. 20017
  Attn: Dr. C. C. Chang

Colorado State University
Fort Collins, Colorado 80521
  Attn: Civil Engineering Hydraulic Laboratory

California Institute of Technology
Pasadena, California 91109
  Attn: Dr. Milton S. Plesset
        Dr. Allan J. Acosta

University of Maryland
College Park, Maryland 20742
  Attn: Dr. Dirse W. Sallet
        Dr. Clifford L. Sayer
        Dr. John D. Anderson

Massachusetts Institute of Technology
Cambridge, Massachusetts 02139
  Attn: Dr. D. R. F. Harleman